# Electron density, electrostatic potential, and spatial organization of ammonium hydrooxalate oxalic acid dihydrate heteromolecular crystal from data of diffraction experiment at 15…

**ARTICLE** *in* RUSSIAN CHEMICAL BULLETIN · AUGUST 2014

Impact Factor: 0.48 · DOI: 10.1007/s11172-013-0252-5



**4 AUTHORS:**

Adam I. Stash
Karpov Institute of Physical Chemistry
**170** PUBLICATIONS **1,308** CITATIONS
SEE PROFILE

Yu-Sheng Chen
University of Chicago
**122** PUBLICATIONS **1,473** CITATIONS
SEE PROFILE

O. V. Kovalchukova
Peoples' Friendship University of Russia
**53** PUBLICATIONS **78** CITATIONS
SEE PROFILE

Vladimir G Tsirelson
Mendeleev Russian University of Chemical Te…
**172** PUBLICATIONS **1,950** CITATIONS
SEE PROFILE

# Electron density, electrostatic potential, and spatial organization of ammonium hydrooxalate oxalic acid dihydrate heteromolecular crystal from data of diffraction experiment at 15 K using synchrotron radiation and theoretical calculations*

*A. I. Stash,[a] Yu-Sheng Chen,[b] O. V. Kovalchukova,[c] and V. G. Tsirelson[d]**

[a]*L. Ya. Karpov Physics and Chemistry Research Institute*
*10 ul. Vorontsovo Pole, 105064 Moscow, Russian Federation.*
*Fax: +7 (495) 917 2490. E-mail: astas@yandex.ru*
[b]*ChemMatCARS Beamline, The University of Chicago Advanced Photon Source,*
*Argonne, Illinois 60439, USA.*
*Fax: +1 (630) 252 0460. E-mail: yschen@cars.uchicago.edu*
[c]*Peoples´ Friendship University of Russia,*
*6 ul. Miklukho-Maklaya, 117198 Moscow, Russian Federation.*
*Fax: +7 (495) 952 2644. E-mail: okovalchukova@mail.ru*
[d]*D. I. Mendeleev University of Chemical Technology of Russia,*
*9 Miusskaya pl., 125047 Moscow, Russian Federation.*
*Fax: +7 (495) 609 2964. E-mail: tsirel@muctr.ru*

A high-precision diffraction study at 15 K using synchrotron radiation and theoretical calculation of a heteromolecular crystal ammonium hydrooxalate oxalic acid dihydrate $NH_4^+ \cdot C_2HO_4^- \cdot C_2H_2O_4 \cdot 2H_2O$ (**1**) were carried out. The calculation was performed with the Kohn—Sham method taking into account periodic boundary conditions. The joint experimental and theoretical study allowed one to locate positions of hydrogen atoms and to reliably establish peculiar features of the electron density and electrostatic potential distributions in **1**. Interatomic and molecular interactions were characterized based on the electron density properties within the framework of a quantum topological theory. The bond order indices were calculated from the experimental electron density without using the orbital notions. A new approach based on visualization of the ellipsoids whose semiaxes depend on the principal values of the electron density curvature at the bond critical points was used. It was found that charge transfer between ammonium cation and hydrooxalate anion in **1** dominates other electrostatic interactions in the crystal. Based on analysis of peculiar features of the electron density and electrostatic potential distributions in the crystal of **1**, it was found that spatial organization of the crystal in hand is also governed by one more, weaker, electrostatic factor that originated from the presence of well-localized regions behind protons on the extensions of the lines of covalent bonds at the periphery of the molecules. In those regions, the electrostatic potential is higher than in other directions due to anisotropy of the electron density distribution. This feature mainly ensures directed complementary electrostatic interaction between corresponding fragments with negatively charged regions of neighboring molecules, such as the lone electron pairs and π-electrons.

**Key words:** electron density, chemical bond, electrostatic interaction.

Studies on the electron density (ED) and electrostatic potential (ESP) distributions in heteromolecular crystals (*i.e.*, crystals with two or more types of independent molecules in the unit cell) make it possible to reveal mechanisms of supramolecular association that occurs through intermolecular interactions of different nature. High-precision X-ray diffraction studies of the ED distribution in such systems are few.[1—8] Theoretical calculations of heteromolecular crystals by the Hartree—Fock and Kohn—Sham methods with allowance for periodic boundary conditions are also scarce.[8]

* Devoted to the memory of our friend and colleague, Corresponding Member of the Russian Academy of Sciences, Professor Mikhail Yuvenal´evich Antipin (1951—2013).

Published in Russian in *Izvestiya Akademii Nauk. Seriya Khimicheskaya,* No. 8, pp. 1752—1763, August, 2013.
1066-5285/13/6208-1752 

In this work, we report on specific features of the ED and ESP distributions in the crystal of ammonium hydrooxalate oxalic acid dihydrate $NH_4^+ \cdot C_2HO_4^- \cdot C_2H_2O_4 \cdot 2H_2O$ (**1**) where different types of chemical bonds coexist. We carried out a high-precision diffraction experiment at 15 K using synchrotron radiation and theoretical calculation of a three-dimensional (3D) crystal in question by the Kohn—Sham method with account for periodic boundary conditions. The joint experimental and theoretical study has made our analysis much more substantiated compared to conventional X-ray diffraction studies of organic compounds. Specific features of chemical bonding in **1** were analyzed using a quantum topological theory of the molecular and crystal structure[9] with inclusion of visualization of certain bonding characteristics. This made it possible to characterize interatomic and molecular interactions of different strength from a unified standpoint based on the electron density properties. It is important that this approach is applicable to both experimentally determined and theoretically calculated electron densities and includes a minimum number of physically substantiated approximations. Also, we analyzed peculiarities of the ESP distribution to study mechanisms of the spatial organization of crystal of **1**.

The synthesis, structure, and properties of compounds containing 2,3,5,6-tetraoxo-4-nitropyridine fragments are of interest[10—13] because their formation involves partial breakdown of the heterocycle to give oxalic acid and its derivatives.[14,15] This also occurs in the presence of strong organic bases. Chemical bonding and intermolecular interactions in the crystal of α-oxalic acid dihydrate were previously thoroughly studied by high-precision X-ray diffraction.[16—18] However, there is only one publication[6] concerning a heteromolecular crystal built of this compound. This is mainly due to difficulties in obtaining single-crystalline specimens suitable for high-precision diffraction experiments.

## Experimental

**Ammonium hydrooxalate oxalic acid dihydrate $NH_4^+ \cdot C_2HO_4^- \cdot C_2H_2O_4 \cdot 2H_2O$ (1)** was obtained upon long-term boiling of aqueous solutions of ammonium 2,3,5,6-tetraoxo-4-nitropyridinate. Single crystals of ammonium 2,3,5,6-tetraoxo-4-nitropyridinate were dissolved in a minimum amount of water, kept in a boiling water bath for 30 min, and then allowed to stay at room temperature for a few days. In the course of natural evaporation of the solvent at room temperature, dark red single crystals of the starting ammonium 2,3,5,6-tetraoxo-4-nitropyridinate and colorless prismatic single crystals of compound **1** were isolated.

A diffraction study using synchrotron radiation was carried out at the ChemMatCARS, Advanced Photon Source (APS) located at Argonne National Laboratory, Illinois, USA. Experimental data were collected at 15 K with a Bruker D8 diffractometer equipped with APEX II CCD detector (diamond (111) monochromator crystal). The specimen was cooled using a Agilent Helijet low-temperature accessory. Reflections were measured using φ-scan technique with an increment of 0.3° at $\lambda = 0.41328$ Å (synchrotron radiation wavelength), detector angles $2\theta = -20°$ and $-40°$, and exposure times of 0.3 and 1.0 s, respectively. The crystal was placed at a distance of 50 mm from the detector.

The diffraction peak intensities were integrated using the APEX II software.[19] The integrated intensities in the data arrays were reduced to a unified scale and averaged using the SORTAV code.[20—22] The structure was solved by the direct method and refined using the full-matrix least-squares method in the anisotropic harmonic approximation for the atomic displacement parameters of nonhydrogen atoms and in the isotropic approximation for hydrogen atoms. Structure determination and refinement of the structural model in the spherical atom approximation were performed using the SHELX97 software package.[23]

Then, we used a multipole structural model.[24] The multipole expansion was truncated at the hexadecapole level for nonhydrogen atoms and at the quadrupole level for H atoms. Since hydrogen atoms are incorrectly located by X-ray analysis, the lengths of all covalent bonds O—H and N—H were fixed on the calculated optimized values (see below). Reliable establishment of disordering of the H atoms involved in strong hydrogen bonds by low-temperature X-ray structural analysis is possible when studying crystals comprised of deuterated molecules. Therefore, in this work the possibility of disordering of the hydrogen atoms involved in the covalent bonds O—H and N—H was left out of consideration. Parameters of the model were refined using the XD2006 program.[25] First, the positions and anisotropic harmonic displacement parameters for nonhydrogen atoms were refined using data for reflections with $\sin\theta/\lambda > 0.8$ Å$^{-1}$. Then, isotropic harmonic displacement parameters for hydrogen atoms were refined using data for reflections with $\sin\theta/\lambda < 0.7$ Å$^{-1}$. Next, the electron multipole populations, the scale factor, and the atomic κ-parameters were refined using the entire data array. Then the approximate multipole structural model was augmented with isotropic secondary extinction parameters according to Becker—Coppens[26] and the refinement procedure was repeated. It was found that extinction in **1** belongs to type 1 and the scatter of the mosaic block orientations can be described by the Lorentz distribution with a parameter value of 15.69″. In the course of the refinement procedure, electroneutrality of the unit cell and non-negativity of the electron density was monitored. Crystallographic data and refinement parameters for structure **1** are listed in Table 1.

The atomic displacement parameters were subject to the Hirshfeld test,[27] for which the mean square amplitudes of atomic displacements of pairs of bonded nonhydrogen atoms perpendicular to the line of the chemical bond should be at most 0.001 Å$^2$. In our case, the scatter of the atomic displacement values ranged from 0 to 0.0004 Å$^2$. The difference Fourier maps of the residual ED that characterize the ED beyond the multipole model and the "noise" in experimental data were calculated using the entire array of reflections and revealed the scatter values ranging from –0.21 to 0.19 e·Å$^{-3}$ at a root-mean-square deviation of 0.05 e Å$^{-3}$. The last-mentioned number can be treated as the estimate of the accuracy in determination of the ED values in this work.

The crystal structure of compound **1** at 15 K (Fig. 1), the atomic positions, and the atomic displacement parameters were

**Table 1.** Experimental details, selected crystallographic data, and refinement parameters for ammonium hydrooxalate oxalic acid dihydrate (**1**)

| Parameter | Value |
|---|---|
| Brutto formula | $C_4H_{11}N_1O_{10}$ |
| $T$/K | 15.0(2.0) |
| Crystal size/mm | 0.07×0.06×0.03 |
| Crystal shape | Prism |
| Wavelength//Å | 0.41328 |
| Space group | $P\bar{1}$ |
| $a$/Å | 6.1997(3) |
| $b$/Å | 7.1894(3) |
| $c$/Å | 10.4452(4) |
| α/deg | 94.659(1) |
| β/deg | 99.758(1) |
| γ/deg | 96.653 (1) |
| $V$/Å$^3$ | 453.31(3) |
| $Z$ | 2 |
| Number of measured reflections | 58907 |
| Number of independent reflections | 12930 |
| Number of reflections with $I > 2\sigma(I)$ | 10650 |
| $R_{int}$ | 0.055 |
| θ/deg | 1.93—31.12 |
| $(\sin\theta/\lambda)_{max}$/Å$^{-1}$ | 1.250 |
| Spherical-atom model (180 parameters) | |
| $R$ | 0.032 |
| $wR$ | 0.085 |
| $S$ | 1.038 |
| Weight scheme, $w$* (spherical model) | |
| $a$ | 0.0488 |
| $b$ | 0.0 |
| $c$ | 0.0 |
| Multipole model (649 parameters, 10121 reflections with $I > \sigma(I)$) | |
| $R$ | 0.0232 |
| $wR$ | 0.316 |
| $S$ | 1.083 |
| Weight scheme, $w$* (multipole model) | |
| $a$ | 0.01 |
| $b$ | 0.0 |
| $c$ | 0.0 |

* $w = (\exp[c(\sin\theta/\lambda)^2])/(\sigma^2(F^2_{obs}) + (ap)^2 + bp)$, where $p = (F^2_{obs} + 2F^2_{calc})/3$ (Sheldrick, 1997).

deposited at the Cambridge Crystallographic Data Center (CCDC 958272 and 958273).

The multipole expansion parameters for crystal **1** were used to calculate the deformation ED (Fig. 2) and the Laplacian of the total ED (Figs 3—5). The ED characteristics at the bond critical points are presented in Table 2. The atomic electron populations were calculated by integrating the total ED over the volumes confined by the surfaces of zero-flux of the ED gradient.[9] The atomic charges estimated from these data to an accuracy of $10^{-5}$ are shown in Fig. 6.

All calculations using experimental ED were carried out with the WinXPRO program.[28,29]

**Computational method.** The three-dimensional crystal of **1** was calculated by the periodic-boundary Kohn—Sham method with the B3LYP hybrid exchange-correlation functional. The 6-311G(d,p) full-electron basis set of Gaussian orbitals has been applied. The CRYSTAL09 program[30] has been used. The Coulomb integrals, the Hartree—Fock exchange integrals, and the exchange-correlation contribution were calculated within the framework of the density functional theory using the default values of the parameters of the CRYSTAL09 program. The admissible levels of energy variations for geometry optimization in the course of the self-consistency procedure and for IR frequency calculations were set to be $1 \cdot 10^{-9}$ and $1 \cdot 10^{-10}$ Hartree, respectively. The number of points in numerical evaluation of the derivatives with respect to nuclear coordinates was 2 and the tolerance factor that specifies the integration grid in the reciprocal space was equal to 4.

During geometry optimization the lattice constants of **1** were fixed on the corresponding experimental values (see Table 1) and only the atomic positions in the unit cell were varied. This approximation gives correct results for the IR intensities and harmonic frequencies in molecular crystals.[31—33] Experimental values of atomic coordinates obtained after refinement of the spherical-atom model were used as the starting point for calculations. Vibrational frequency calculations at the Γ point gave positive values; this confirms that the optimized structure of **1** corresponds to a minimum on the potential energy surface.

The calculated bond length values are listed in Tables 2 and 3. The lengths of the covalent bonds involving hydrogen atoms were used as fixed parameters in the refinement of the multipole structural model with the data of the diffraction experiment using synchrotron radiation (see above).

## Results and Discussion

**Geometric parameters.** In the crystal of **1**, fragments comprised of two independent oxalic acid molecules, the hydrooxalate anion, and two independent water molecules linked by hydrogen bonds O—H...O form infinite chains along the [011] direction (see Fig. 1). From geometric considerations, three O—H...O hydrogen bonds can be treated as strong ones; indeed, the O(1)...O(10), O(3)...O(5), and O(7)...O(9) distances are 2.492, 2.480, and 2.451 Å, respectively. The chains form a three-dimensional network through weak hydrogen bonds O—H...O and N—H...O that are formed by water molecules and ammonium cations.

In the text below we will discuss both types of bond length values, namely, experimental distances for pairs of nonhydrogen atoms and the results of theoretical calculations of the crystal of **1** for the O—H, N—H, and O...H bonds. This makes it possible to eliminate errors in the location of H atoms that are intrinsic in X-ray diffraction. It should be noted that for pairs of nonhydrogen atoms the internuclear distances coincide with the results of calculations (see Table 2) up to a root-mean-square deviation and agree well with the data of room-temperature experimental studies of the crystal of **1** by neutron diffraction[34] and X-ray diffraction.[35] Our experiment carried out at 15 K gave the following lengths of the formally double bonds C=O in the oxalic acid molecules: 1.225 Å for

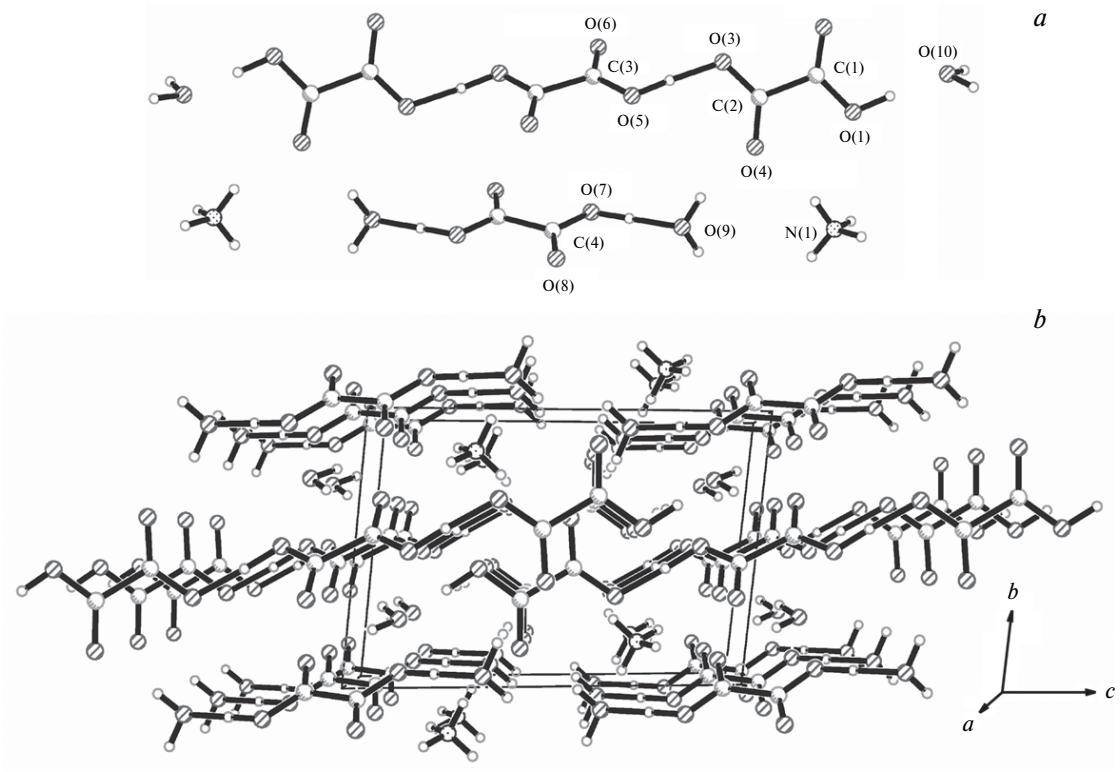


**Fig. 1.** Crystal structure of **1**: general view along the *a* axis (*a*) and a fragment of infinite chain of molecules along the [011] direction (*b*).

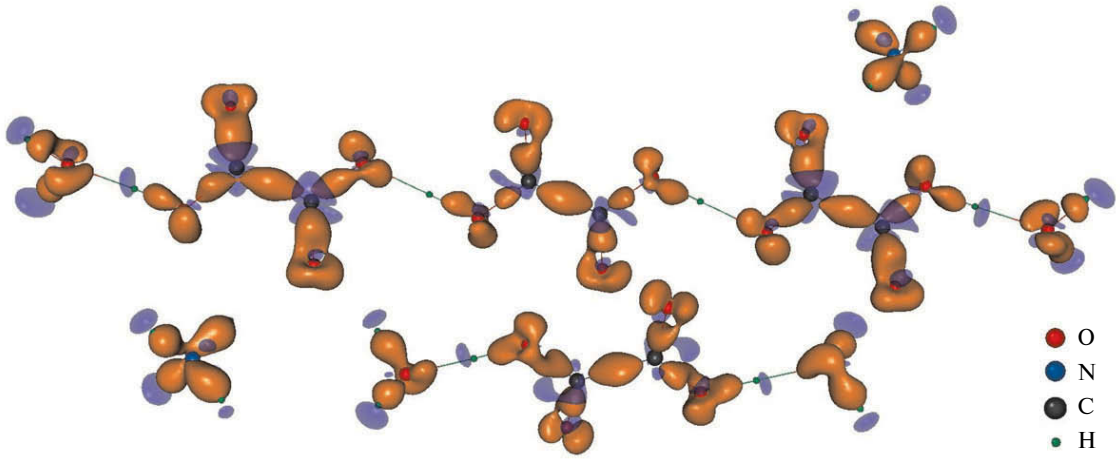


**Fig. 2.** Visualization of the 3D deformation electron density in the crystal of **1**. Regions with the excess electron density $\delta\rho = 0.3$ e Å$^{-3}$ and regions depleted of electron density $\delta\rho = -0.2$ e Å$^{-3}$ are shown in orange and blue, respectively.
*Note*. Figures 2—7 are available in full color in the on-line version of the journal (http://www.springerlink.com).

C(3)=O(6) and 1.221 Å for C(4)=O(8). The lengths of the corresponding bonds in the hydrooxalate anion are 1.222 Å for C(1)=O(2) and 1.243 Å for C(2)=O(4). The C—O(H) bond lengths in these fragments are as follows: C(1)—O(1) 1.294, C(3)—O(5) 1.283, and C(4)—O(7) 1.286 Å. These distances differ from conventional values[36] of 1.200 Å for C=O and 1.360 Å for C—O(H) (see below).

In the hydrooxalate anion, the bonds C(2)—O(3) and C(2)—O(4) have close lengths of 1.258 and 1.243 Å, respectively. The difference between them is probably due to different degrees of hydrogen bonding.

Ammonium cations have the shape of distorted tetrahedra with the HNH angles lying between 107.0 and 111.3°. The N—H bond lengths fixed on the theoretical-

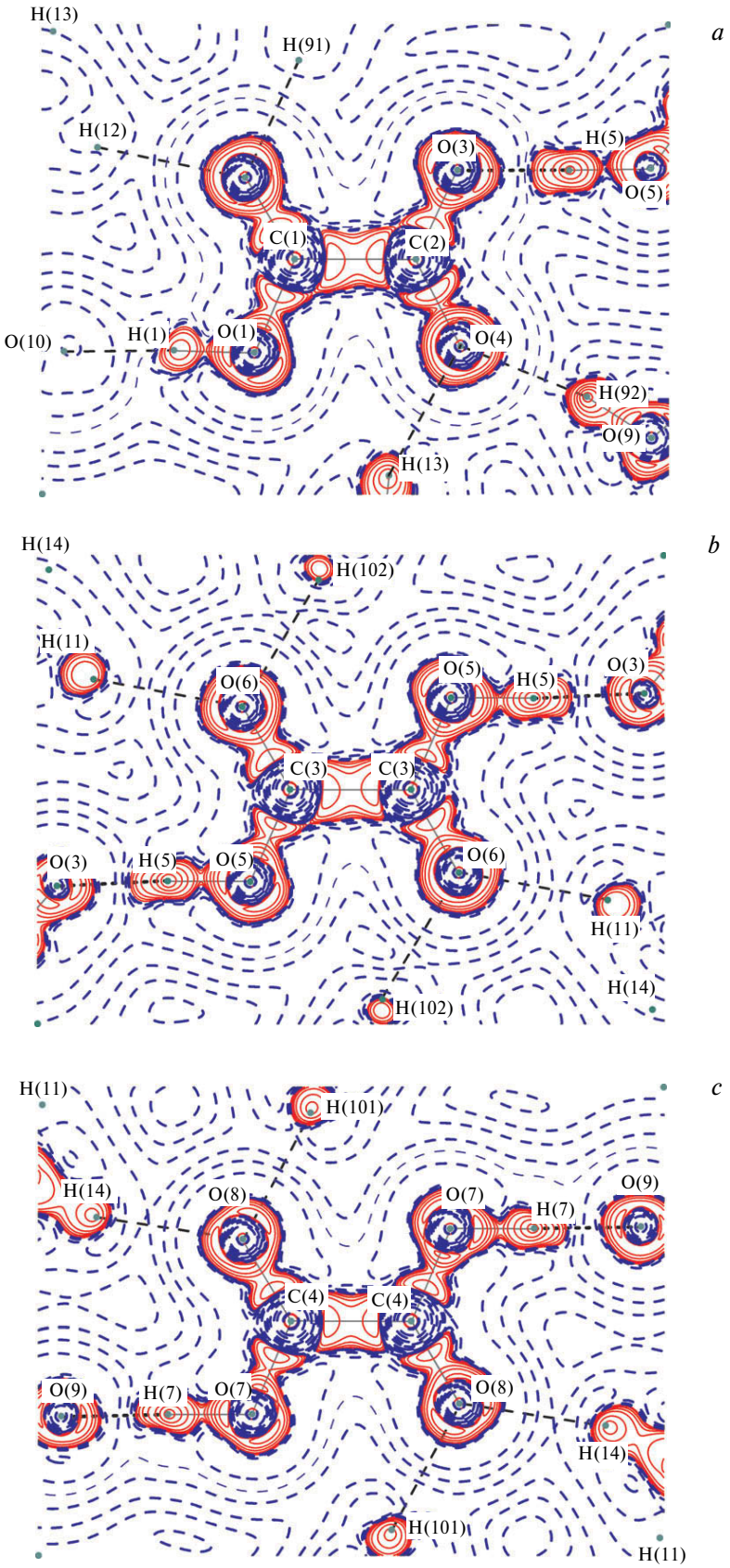


**Fig. 3.** Contour maps of the Laplacian of the total electron density in the plane passing through independent oxalic acid molecules (*a*, *b*) and hydrooxalate anion (*c*). Here and in Figs 4 and 5 dashed lines are drawn with increments of $2 \cdot 10^n$, $4 \cdot 10^n$, and $8 \cdot 10^n$ e Å$^{-5}$ ($-3 \le n \le 3$); solid lines correspond to negative values of the Laplacian of the electron density.

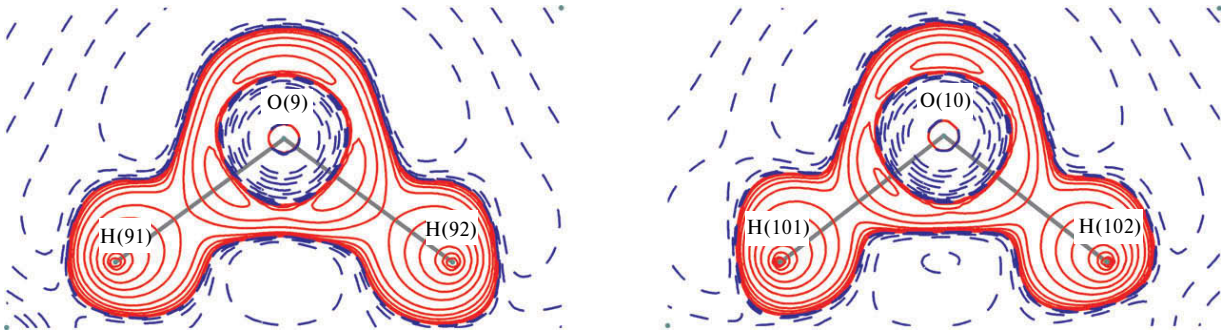


**Fig. 4.** Contour maps of the Laplacian of the total electron density for two independent water molecules in the H—O—H plane.

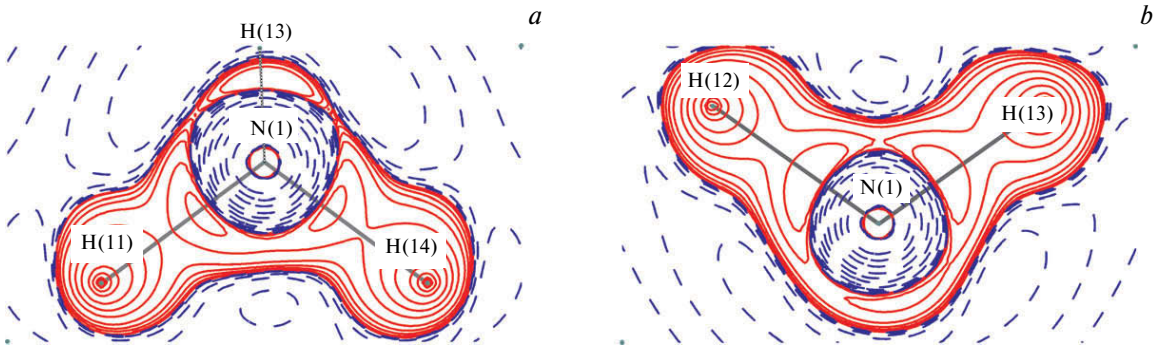


**Fig. 5.** Contour maps of the Laplacian of the total electron density in two mutually perpendicular planes passing through the H(11)—N(1)—H(14) (*a*) and H(12)—N(1)—H(13) (*b*) atoms of ammonium ion.

ly determined values (see Table 2) are in the range 1.025—1.033 Å (*cf.* 0.995—1.022 Å for the corresponding bond lengths reported in the neutron diffraction study[34]).

**Atomic charges and bond-order indices.** Within the framework of the orbital approach, specific features of chemical bonding are often described using the model of atomic charges and the bond order indices.[37] These notions are widely used in chemistry; therefore, it is important to obtain a similar description in terms of the electron density. For atomic charges, this problem was solved by Bader two decades ago,[9] namely, the atomic electron populations $N_i$ are calculated by integrating the total ED over regions confined by the surfaces of the zero-flux of the gradient of the electron density and the atomic charges are evaluated as $Q_i = Z_i - N_i$. These values are presented in Fig. 6.

Recently, a quite correct unified description of the bond orders for covalent and hydrogen bonds within the framework of a quantum topological theory was reported. In particular, the authors of Refs 38 and 39 embodied the idea[40] of approximating the Cioslowski—Mixon bond orders[41] by the expression

$$n_{topo} = a_0 + a_1\rho(\mathbf{r}_b) + a_2(\lambda_1 + \lambda_2) + a_3\lambda_3, \qquad (1)$$

where $\rho(\mathbf{r}_b)$ are the electron density values at bond critical points (BCPs) and $\lambda_1$, $\lambda_2$, and $\lambda_3$ are the electron density curvatures at the BCPs. The coefficients $a_i$ were determined in Refs 38 and 39. Table 2 presents the bond-order indices for compound **1** calculated using expression (1).

The calculated atomic charges enable evaluation of "pure" charge transfer between fragments in the heteromolecular crystal of **1**. Summation over atoms shows that ammonium cation $NH_4^+$ bears a charge of +0.89 e, whereas the hydrooxalate anion $C_2O_4H^-$ has an excess electron charge of –0.82 e while the oxalic acid molecules bear charges of –0.12 and –0.26 e. Independent water molecules have charges of –0.03 and +0.11 e. Therefore, electron charge in the crystal is mainly transferred from ammonium cation to the hydrooxalate anion while the oxalic acid molecules bear only a small negative charge. This is in good agreement with the results obtained from the electron density values in previous studies on charge transfer in other heteromolecular complexes.[8]

The bond order indices listed in Table 2 suggest that all C—C bonds in the crystal of **1** are similar to ordinary bonds. The orders of the formally double bonds C=O in the oxalic acid molecules are close to 1.5. This agrees well with the corresponding internuclear distances that are longer than conventional double bonds.[36] However, it should be noted that the corresponding Pauling bond orders calculated from internuclear distances are only 1.36—1.38. The orders of the formally ordinary bonds

**Table 2.** Characteristics of bond critical points in the crystal ammonium hydrooxalate oxalic acid dihydrate (**1**)

| Bond* | $\rho_b$ | $\nabla^2\rho$ | *R* | *d*1 | *d*2 | $-\lambda_1$ | $-\lambda_2$ | $\lambda_3$ | Bond order (4) |
|---|---|---|---|---|---|---|---|---|---|
| | e Å$^{-5}$ | | Å | | | e Å$^{-5}$ | | | |
| O(1)—C(1) | 2.554 | −34.56 | 1.294 | 0.805 | 0.489 | 4.06 | 22.06 | 11.56 | 1.32 |
| O(1)—H(1) | 1.842 | −39.95 | 1.040 | 0.835 | 0.206 | 31.66 | 29.65 | 21.39 | 0.60 |
| O(2)—C(1) | 3.055 | −38.42 | 1.222 | 0.784 | 0.439 | 30.64 | 27.79 | 20.01 | 1.59 |
| O(3)—C(2) | 2.725 | −35.32 | 1.258 | 0.801 | 0.458 | 27.22 | 23.92 | 15.82 | 1.38 |
| O(4)—C(2) | 2.934 | −35.59 | 1.243 | 0.758 | 0.485 | 26.97 | 24.22 | 15.61 | 1.64 |
| O(5)—C(3) | 2.433 | −26.99 | 1.283 | 0.816 | 0.467 | 22.95 | 18.31 | 14.27 | 1.27 |
| O(5)—H(5) | 1.739 | −31.46 | 1.055 | 0.836 | 0.220 | 28.97 | 27.13 | 24.65 | 0.41 |
| O(6)—C(3) | 2.899 | −33.22 | 1.225 | 0.786 | 0.440 | 28.18 | 24.98 | 19.94 | 1.52 |
| O(7)—C(4) | 2.509 | −31.01 | 1.286 | 0.808 | 0.479 | 24.03 | 19.88 | 12.90 | 1.31 |
| O(7)—H(7) | 1.651 | −31.20 | 1.079 | 0.857 | 0.223 | 27.80 | 24.91 | 21.50 | 0.51 |
| O(8)—C(4) | 2.788 | −27.39 | 1.221 | 0.787 | 0.434 | 27.77 | 22.84 | 23.22 | 1.41 |
| O(9)—H(91) | 2.342 | −66.09 | 0.980 | 0.794 | 0.186 | 44.61 | 43.88 | 22.40 | 0.81 |
| O(9)—H(92) | 2.375 | −62.98 | 0.981 | 0.794 | 0.187 | 44.37 | 43.69 | 25.02 | 0.69 |
| O(10)—H(101) | 2.346 | −59.16 | 0.974 | 0.777 | 0.198 | 42.83 | 39.58 | 23.28 | 0.72 |
| O(10)—H(102) | 2.409 | −61.20 | 0.973 | 0.765 | 0.208 | 42.46 | 40.46 | 21.72 | 0.79 |
| N(1)—H(11) | 2.178 | −30.52 | 1.025 | 0.743 | 0.282 | 27.85 | 25.92 | 23.24 | 0.84 |
| N(1)—H(12) | 2.213 | −43.83 | 1.027 | 0.800 | 0.227 | 33.19 | 32.89 | 22.25 | 0.61 |
| N(1)—H(13) | 2.228 | −39.68 | 1.033 | 0.782 | 0.251 | 31.07 | 30.98 | 22.37 | 0.71 |
| N(1)—H(14) | 2.210 | −34.08 | 1.028 | 0.746 | 0.282 | 28.47 | 27.47 | 21.85 | 0.83 |
| C(1)—C(2) | 1.752 | −13.68 | 1.550 | 0.793 | 0.757 | 13.73 | 11.76 | 11.81 | 0.88 |
| C(3)—C(3)$^{i}$ | 1.763 | −13.91 | 1.546 | 0.773 | 0.773 | 13.59 | 11.83 | 11.51 | 0.88 |
| C(4)—C(4)$^{ii}$ | 1.724 | −13.29 | 1.536 | 0.768 | 0.768 | 13.80 | 10.74 | 11.25 | 0.91 |
| O(3)...H(5) | 0.787 | −2.57 | 1.428 | 0.983 | 0.445 | 7.41 | 6.83 | 11.67 | 0.28 |
| O(9)...H(7) | 0.783 | −2.52 | 1.372 | 0.983 | 0.391 | 8.17 | 7.06 | 12.71 | 0.26 |
| O(10).....H(1) | 0.551 | 1.56 | 1.457 | 1.035 | 0.427 | 5.04 | 4.18 | 10.79 | 0.18 |
| O(2)...H(91)$^{iii}$ | 0.247 | 1.83 | 1.749 | 1.174 | 0.576 | 1.72 | 1.65 | 5.20 | 0.09 |
| O(4)...H(92) | 0.275 | 2.07 | 1.739 | 1.153 | 0.588 | 1.92 | 1.75 | 5.74 | 0.10 |
| O(8)...H(101)$^{iv}$ | 0.206 | 1.42 | 1.840 | 1.208 | 0.635 | 1.46 | 1.12 | 4.01 | 0.08 |
| O(6)...H(102)$^{v}$ | 0.150 | 1.01 | 1.913 | 1.269 | 0.669 | 0.97 | 0.83 | 2.81 | 0.06 |
| O(6)...H(11)$^{vi}$ | 0.132 | 1.94 | 1.944 | 1.258 | 0.688 | 0.80 | 0.63 | 3.37 | 0.05 |
| O(2)...H(12)$^{iii}$ | 0.153 | 1.75 | 1.955 | 1.247 | 0.710 | 0.89 | 0.76 | 3.40 | 0.06 |
| O(4)...H(13) | 0.182 | 1.81 | 1.895 | 1.224 | 0.679 | 1.14 | 1.00 | 3.96 | 0.07 |
| O(8)...H(14)$^{vii}$ | 0.144 | 2.04 | 1.897 | 1.240 | 0.658 | 0.87 | 0.83 | 3.75 | 0.05 |

*Note:* $\rho_b$ and $\nabla^2\rho$ are the electron density and the Laplacian of the electron density at the bond critical point; *R* is the internuclear distance; *d*1 (*d*2) are the distances from the first (second) atom of the A—B bond to the bond critical points; $\lambda_1$, $\lambda_2$ and $\lambda_3$ are the electron density curvatures at the bond critical points.

* Symmetry transformations: (i) $1-x, 1-y, -z$; (ii) $1-x, 2-y, -z$; (iii) $x, -1+y, z$; (iv) $x, 1+y, -1+z$; (v) $-1+x, y, -1+z$; (vi) $1-x, 1-y, -z$; (vii) $2-x, 2-y, 1-z$.

C(3)—O(5) and C(4)—O(7) are 1.27—1.31. The orders of the C(1)=O(2) and C(2)=O(4) bonds in the hydrooxalate anion are 1.59 and 1.64, respectively; *i.e.*, the latter bond to a greater extent resembles a double bond. These parameters suggest that the electron density in the crystal of **1** is delocalized over O—C=O fragments of the oxalic acid molecules and hydrooxalate anions; as a result, the orders of the formally double bonds C=O decrease while those of the formally ordinary bonds increase. This conclusion can be well illustrated by a three-dimensional image of the deformation ED (see Fig. 2) which shows that the ED of the lone electron pairs of oxygen atoms is connected to the ED on covalent bonds in the O—C=O fragment through bridges. This reflects electron delocalization over the molecules. An analysis of the maps of the Laplacian of the electron density leads to the same conclusion (see Figs 3—5).

The lengths of the covalent bonds O—H whose hydrogen atoms are involved in strong hydrogen bonds vary from 1.040 to 1.079 Å. The corresponding bond orders lie between 0.41 and 0.60. The orders of the covalent bonds O—H (0.973—0.971 Å long) and N—H (1.025—1.033 Å long) with the H atoms involved in weak hydrogen bonds are 0.69—0.71 and 0.60—0.84, respectively.

The orders of strong H-bonds lie in the range 0.18—0.28, those of weak H-bonds are 0.06—0.10 for the bonds involving water molecules and 0.05—0.07 for the bonds involving ammonium molecules.

**Table 2.** Covalent bond lengths in compound **1**

| Bond* | *d*/Å | |
|---|---|---|
| | Experiment | Calculations |
| C(1)—O(1) | 1.294(3) | 1.300 |
| C(2)—O(3) | 1.258(3) | 1.254 |
| C(2)—O(4) | 1.243(3) | 1.224 |
| C(3)—O(5) | 1.283(3) | 1.288 |
| C(3)—O(6) | 1,225(3) | 1.225 |
| C(4)—O(7) | 1.286(3) | 1.289 |
| C(4)—O(8) | 1.221(3) | 1.225 |
| C(1)—C(2) | 1.550(3) | 1.554 |
| C(3)—C(3)$^{i}$ | 1.546(4) | 1.547 |
| C(4)—C(4)$^{ii}$ | 1.537(4) | 1.541 |

* Symmetry transformations: (i) $1-x$, $1-y$, $-z$; (ii) $1-x$, $2-y$, $-z$.

The energies of weak hydrogen bonds (O)H...O and (N)H...O can be evaluated using the kinetic energy density $g_b$ at corresponding BCPs *via* the relation[42] $E_H = 0.429\, g_b$. This expression proved itself for $E_H < 85$ kJ mol$^{-1}$ (R(H...O) > 1.40 Å).[33–43] We determined the energies $E_H$ using the Kirzhnits relation[44] for calculating the $g_b$ values from the experimental electron density and the Laplacian of the electron density $\nabla^2\rho(\mathbf{r}_b)$ at the BCP. It was found that the average energies of (O)H...O and (N)H...O bonds are about 31 and 26 kJ mol$^{-1}$, respectively. This agrees with the corresponding hydrogen bond orders (see above).

Therefore, the bond orders calculated from experimental electron density using expression (1) make it possible to qualitatively assess the strengths of covalent and hydrogen bonds and even to rank same-type bonds without using the orbital approach.

**Visualization of quantum topological characteristics of chemical bonding.** The character of electron localization in the coordinate space predetermines the type and specific features of chemical bonding. Localization is related to the electron kinetic energy density and depends on the squared electron momentum. In quantum mechanics, by virtue of the Heisenberg uncertainty principle, exact values of the coordinate **r** and the local momentum of an electron in the coordinate representation can not be determined simultaneously. However, a local statistical quantum theory[45] shows that, having specified an exact value of the variable **r**, one can get the following local expression for the average electron momentum in the coordinate representation[46]:

$$\boldsymbol{p}(\mathbf{r}) = -0.5\nabla\rho(\mathbf{r})/\rho(\mathbf{r}) \qquad (2)$$

(here, the system of atomic units is used: h = 1, $m$ = 1, $e$ = 1; $\rho(\mathbf{r})$ is the electron density).

Isocontours of the scalar function $p(\mathbf{r}) = -0.5|\nabla\rho(\mathbf{r})|/\rho(\mathbf{r})$ in the vicinity of critical points of the electron density $\mathbf{r}_0$ (at which the gradient of the electron density $\nabla\rho(\mathbf{r}\rightarrow\mathbf{r}_0)$ approaches zero) form certain figures characterizing the electron density curvature.[47,48] We dwell on them in more detail. Let us present the gradient of the electron density near the BCP $(x_0, y_0, z_0)$ as follows[48]:

$$\nabla\rho(\mathbf{r}_0) \approx (x-x_0)\lambda_1\mathbf{u}_1 + (y-y_0)\lambda_2\mathbf{u}_2 + (z-z_0)\lambda_3\mathbf{u}_3, \qquad (3)$$

where $\lambda_{1,2,3}$ are the principal values of the 3×3 Hesse matrix of the electron density, $\mathbf{u}_{1,2,3}$ are the orthonormalized

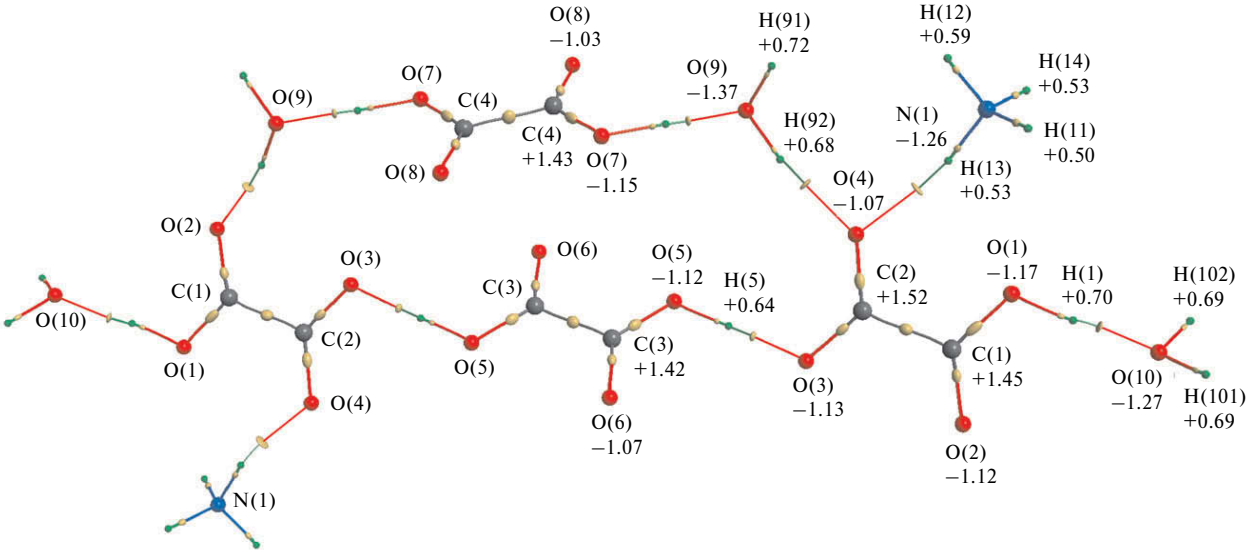


**Fig. 6.** Fragment of the crystal structure of **1**. Shown are the charges on symmetrically independent atoms (for the description of the method for evaluation of atomic charges, see text). Atoms are connected by the bond lines; shown are the rotation ellipsoids that visually characterize the topology of the electron density distribution around the critical points of covalent and hydrogen bonds.

eigenvectors of this matrix at points $\mathbf{r}\rightarrow\mathbf{r}_0$. Taking the square of expression (2) and dividing both sides of the equation by $|\nabla\rho|^2$, one gets a canonical equation of an ellipsoid centered at $\mathbf{r}_0$

$$((x-x_0)^2/a^2 + (y-y_0)^2/b^2 + (z-z_0)^2/c^2) = 1. \qquad (4)$$

The principal semiaxes of the ellipsoid are $a = \nabla\rho/\lambda_1$, $b = \nabla\rho/\lambda_2$, and $c = \nabla\rho/\lambda_3$. However, since the gradient of the electron density at the critical point is zero, it is recommended that the lengths of the semiaxes of the ellipsoid (4) be represented in alternative manner[48]:

$$a = 3\rho[(|\lambda_1|\cdot|\lambda_2|\cdot|\lambda_3|)^{1/6}/4|\lambda_1|],$$

$$b = 3\rho[(|\lambda_1|\cdot|\lambda_2|\cdot|\lambda_3|)^{1/6}/4|\lambda_2|],$$

$$c = 3\rho[(|\lambda_1|\cdot|\lambda_2|\cdot|\lambda_3|)^{1/6}/4|\lambda_3|].$$

Therefore, isocontours of the function $p(\mathbf{r})$ surrounding BCPs represent ellipsoids centered at the BCPs. Semiaxes of the ellipsoids are aligned to the principal directions of the Hesse matrix, *i.e.*, the three principal directions of the electron density curvature. It follows that the shape of the surfaces of these figures specified by Eq. (4) characterizes the topological properties of the electron density. At BCPs and at points on the bond lines,[48] the ellipsoid given by expression (4) is a graphical representation of different types of interatomic interactions.[48] Now we will apply this feature to describe interatomic interactions in the crystal of **1**.

At the critical points of the covalent bonds C—O, O—H, and N—H, one has $\lambda_3 < |\lambda_1|,|\lambda_2|$. It follows that $c > a,b$ and corresponding ellipsoids should be extended along the bond lines. Indeed, it is just such figures (see Fig. 6) that were observed in the region of these bonds in the crystal of **1**. Ellipsoids on the covalent bonds C—O are more extended along the *c* axis, those on the O—H and N—H bonds are less extended along the *c* axes, while ellipsoids on the C—C bonds are close to spheres. This makes C—C bonds in compound **1** close to a specific kind of covalent bonds called the charge shift bonds for which the charge is displaced from the internuclear space toward atomic cores.[49]

For hydrogen bonds (noncovalent interactions similar to closed-shell ones), one has $\lambda_3 > |\lambda_1|,|\lambda_2|$, *i.e.*, $c < a,b$ (see Table 2) and the ellipsoid is transformed to a disc whose plane is perpendicular to the bond line (see Fig. 6). A comparison of the size of the disc and the lengths and bond-order indices of the H-bonds reveals that weaker N—H bonds correspond to discs with larger radii.

Ellipsoids (4) for ring and cage critical points of the electron density are omitted for clarity. Mention may only be made that at a ring critical point, one has $a \approx b < c$ and both disc-shaped and spindle-shaped figures can be observed depending on the ratio of the electron density curvature parameters. For the ellipsoids at cage critical points, one has $a \approx b \approx c$ and the figures resemble spheres.

Our approach, which is based on visualization of expression (4), makes the quantum topological properties of chemical bonds as clear as possible and simplifies a direct visual comparison. Also, it is at least equally important that this approach describes chemical bonding better than the canonical quantum topological structural theory by Bader[9] because critical points of the electron density are characterized by not only the signs of three values of the electron density curvature along the principal directions at BCPs, but also by their absolute values.

**Specific features of the electron density and electrostatic potential and the spatial organization of the crystal of 1.** Charge transfer between ammonium cation and hydrooxalate anion dominates among electrostatic interactions in the crystal of **1**. However, an analysis of peculiar features of the electron density and electrostatic potential distribution also allows one to study weaker mechanisms of the spatial organization of the crystal of **1**. Let us divide the crystal into constituent molecular fragments; this can be done with ease using the multipole model (relevant maps are omitted). It appears that the ESP of atomic nuclei makes the major contribution to the potential around the ammonium ion. The same picture is also observed behind protons outside other molecules, while the contributions of the lone electron pairs to the ESP form local regions having relatively lower potentials with local minima near O atoms of other molecules. (It should be recalled that the ESP is defined up to a constant and it is physically correct to consider the potential differences at different points of space). A comparison of the complementary regions of the total ESP around particular molecular fragments "isolated" from the crystal and the pattern of the bond lines for noncovalent interactions suggests that the spatial organization of the heteromolecular crystal of **1** also depends on electrostatic interactions originated from the network of hydrogen bonds. First of all, look at the differences in details of the ESP distribution for strong and weak hydrogen bonds. The nuclei of all H atoms involved in the strong hydrogen bonds O(1)...O(10), O(3)...O(5), and O(7)...O(9) lie within strips of negative values of the Laplacian of the electron density extended along the O...O contacts. In these regions, the electron density is concentrated. It is important that these strips penetrate regions adjacent to the O atoms involved in the H-bonds so deeply that positions of the critical points of the O(3)...H(5) and O(9)...H(7) bonds appear within them (see Table 2). Consequently, there is some covalent contribution to strong H-bonds.[33,50,51] In contrast, nuclei of the H atoms involved in weak hydrogen bonds are located near boundaries of the regions of negative values of the ED Laplacian that mainly lie on the covalent bonds O—H and N—H (see Figs 3—5). For both types of hydrogen bonds, electrostatic field of H nuclei is more

shielded along the O—H covalent bonds than along the H...O contacts.

Judging from the deformation electron density maps (see Fig. 2) and the Laplacian of the electron density maps (see Figs 3, 5), the oxygen atoms of oxalic acid molecules, hydrooxalate anion, and water molecules involved in strong hydrogen bonds can be treated as being nearly $sp^3$-hybridized. These atoms do not form other hydrogen bonds and their lone electron pairs are involved in the formation of a general pattern of undirected inner-crystal electrostatic and dispersion interactions in the crystal of **1**. Other oxygen atoms are $sp^2$-hybridized and their lone electron pairs are involved in weak H-bonds. By and large, oxygen atoms in the crystal of **1** retain hybridizations typical of the O atoms in corresponding constituent molecules; only peripheral regions of the lone electron pairs with different degree of perturbation are involved in H-bonding in the crystal.

Nonuniform electron density distribution in the molecules leads to anisotropic shielding of positive charges of atomic nuclei by electrons along different radial directions. In particular, terminal H atoms of molecules in compound **1** are involved in covalent σ-bonds and the electron density of these atoms is partially displaced toward intramolecular regions of internuclear space (see Fig. 2). Because of this, well-localized regions of negative deformation electron density appear behind the nuclei at the periphery of the molecules on extensions of the lines of covalent bonds. As a result, regions with higher electrostatic potential compared to the ESP along other directions appear here. These regions resemble positive σ-holes observed in halogen bonds.[52,53] Although having another nature, they also ensure complementary electrostatic interaction between corresponding fragments and negatively charged fragments of neighboring molecules, such as lone electron pairs and π-electrons. This interaction is part of the overall electrostatic intermolecular interaction and mainly has a directed character.[54,55]

Clearly, regions with higher and lower ESP are less pronounced in crystals compared to single molecules owing to mutual penetration of the electron clouds of neighboring molecules. Nevertheless, "fingerprints" of the regions with relatively high ESP are clearly seen in the crystal of **1** (Fig. 7). For both strong and weak hydrogen bonds, higher ESP values were found at the periphery of all molecules on extensions of the lines of the covalent bonds N—H and O—H. Regions with relatively higher ESP values are oriented along the lines of hydrogen bonds toward the lone electron pairs of O atoms. Noteworthy is that for strong H-bonds the electron density isosurface $\rho = 0.1$ e Å$^{-3}$ corresponding to less negative ESP values is noticeably extended along the lines of O...H bonds, whereas for weak H-bonds this feature is much less pronounced. Also, the "cap" of the higher ESP for weak hydrogen bonds is more diffuse along the directions perpendicular to the bond lines. This observation supports the idea of greater directionality of strong hydrogen bonds. A comparison of the size of the ESP "cap" for the weak H-bonds N...H and O...H suggests that the hydrogen bonds formed by ammonium cation are characterized by somewhat lower directionality. This agrees with the conclusions that these bonds in the crystal of **1** are weaker than other bonds (see above).

Summing up, in this work, we exactly located positions of hydrogen atoms and reliably determined specific features of the electron density and electrostatic potential distribution in the heteromolecular crystal $NH_4^+ \cdot C_2HO_4^- \cdot \cdot C_2H_2O_4 \cdot 2H_2O$ (**1**) using data of high-precision diffraction experiment using synchrotron radiation at 15 K and the results of theoretical calculations by the Kohn—Sham method with inclusion of periodic boundary conditions. Different types of interatomic and molecular interactions were characterized based on the properties of the electron

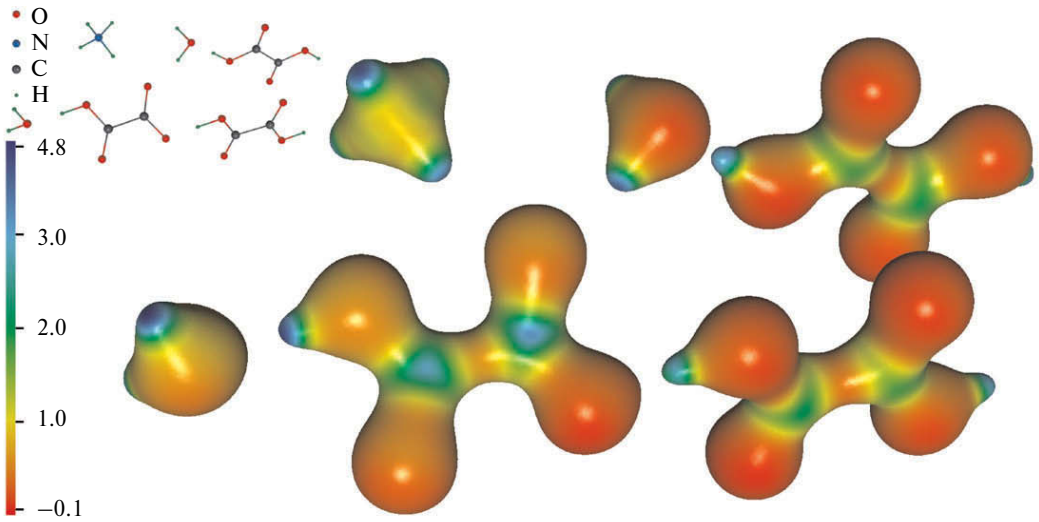


**Fig. 7.** Spatial distribution of electrostatic potential on the electron density isosurface $\rho = 1.0$ e • Å$^{-3}$ in a fragment of the crystal of **1**.

density. It was established that charge transfer between ammonium cation and hydrooxalate anion dominates in the crystal of **1** and that water and oxalic acid molecules bear only small negative charges. The bond-order indices calculated from the experimental electron density made it possible to evaluate the strength of covalent and hydrogen bonds and to rank same-type bonds without using the orbital approximation. The new approach realized in this work is free from any approximation, being based on visualization of ellipsoids whose semiaxes depend on the principal values of the electron density curvature at bond critical points. This makes the quantum topological characteristics of chemical bonds as clear as possible and simplifies a direct visual comparison. Our approach also provides a comprehensive description of chemical bonding because critical points of the electron density are characterized by both the signs and absolute values of the electron density curvature along the principal directions at BCPs.

An analysis of specific features of the electron density and electrostatic potential distribution allowed mechanisms of spatial organization of the crystal of **1** to be studied. In addition to electrostatic interaction between differently charged molecular fragments there is one more, weaker, factor of electrostatic interaction, *viz.*, well-localized regions behind protons at the periphery of molecules on extensions of the lines of covalent bonds. The electrostatic potential in these regions is higher than along other directions. These complementary regions provide an additional, mainly directed, electrostatic interaction between corresponding fragments and negatively charged fragments of neighboring molecules.

The authors express their gratitude to E. V. Bartashevich for fruitful advice during the preparation of the manuscript.

This work was financially supported by the Russian Foundation for Basic Research (Project No. 13-03-00767-a). Use of the Advanced Photon Source was financially supported by the US Department of Energy, Office of Science, Office of Basic Energy Sciences, under Contract No. DE-AC02-06CH11357. ChemMatCARS Sector 15 is principally supported by the National Science Foundation/US Department of Energy under Grant No. NSF/CHE-0822838.

## References

1. D. G. Golovanov, K. A. Lyssenko, M. Yu. Antipin, Ya. S. Vygodskii, E. I. Lozinskaya, A. S. Shaplov, *Cryst. Growth Des.*, 2005, **5**, 337.
2. K. A. Lyssenko, D. G. Golovanov, V. I. Meshcheryakov, A. R. Kudinov, M. Yu. Antipin, *Russ. Chem. Bull.* (*Int. Ed.*), 2005, **54**, 933 [*Izv. Akad. Nauk, Ser. Khim.*, 2005, 911].
3. E. Espinosa, E. Molins, C. Lecomte, *Phys. Rev. B: Condens. Matter*, 1997, **56**, 1820.
4. A. O. Borissova, A. A. Korlyukov, M. Yu. Antipin, K. A. Lyssenko, *J. Phys. Chem. A*, 2008, **112**, 11519.
5. K. A. Lyssenko, P. Yu. Barzilovich, Yu. V. Nelyubina, E. A. Astaf´ev, M. Yu. Antipin, S. M. Aldoshin, *Russ. Chem. Bull.* (*Int. Ed.*), 2009, **58**, 31 [*Izv. Akad. Nauk, Ser. Khim.*, 2009, 31].
6. E. M. Schmidtmann, L. J. Farrugia, D. S. Middlemiss, M. J. Gutmann, G. J. McIntyre, C. C. Wilson, *J. Phys. Chem.*, 2009, **113**, 13985.
7. E. A. Zhurova, A. Martin, A. A. Pinkerton, *J. Am. Chem. Soc.*, 2002, **124**, 8741.
8. E. A. Zhurova, V. G. Tsirelson, A. I. Stash, M. V. Yakovlev, A. A. Pinkerton, *J. Phys. Chem.*, 2004, **108**, 20173.
9. R. F. W. Bader, *Atoms in Molecules: A Quantum Theory*, Oxford Univ. Press, Oxford—New York, 1994, 458 pp.
10. K. K. Palkina, N. E. Kuz´mina, O. V. Koval´chukova, S. B. Strashnova, B. E. Zaitsev, *Dokl. Chem.* (*Engl. Transl.*), 2000, **370**, 26 [*Dokl. Akad. Nauk*, 2000, **370**, 631].
11. O. V. Koval´chukova, S. B. Strashnova, B. E. Zaitsev, K. K. Palkina, S. V. Nikitin, in *Novye dostizheniya v khimii karbonil´nykh i geterotsiklicheskikh soedinenii* [*Advances in Chemistry of Carbonyl and Heterocyclic Compounds*], Saratovskii Gos. Univ., Saratov, 2000, p. 108 (in Russian).
12. O. V. Koval´chukova, S. B. Strashnova, B. E. Zaitsev, M. A. Ryabov, N. E. Kuz´mina, K. K. Palkina, *Russ. J. Inorg. Chem.* (*Engl. Transl.*), 2003, **48**, 194 [*Zh. Neorgan. Khim.*, 2003, **48**, 244].
13. N. E. Kuz´mina, O. V. Koval´chukova, S. B. Strashnova, K. K. Palkina, B. E. Zaitsev, N. Yu. Isaeva, *Crystallogr. Rep.* (*Engl. Transl.*), 2004, **49**, 758 [*Kristallografiya*, 2004, **49**, 847].
14. K. K. Palkina, N. E. Kuz´mina, O. V. Koval´chukova, S. B. Strashnova, B. E. Zaitsev, *Russ. J. Inorg. Chem.* (*Engl. Transl.*), 2001, **46**, 1495 [*Zh. Neorgan. Khim.*, 2001, **46**, 1492].
15. O. V. Koval´chukova, B. E. Zaitsev, S. B. Strashnova, N. E. Kuz´mina, K. K. Palkina, *Dokl. Chem.* (*Engl. Transl.*), 2002, **386**, 251 [*Dokl. Akad. Nauk*, 2002, **386**, 645].
16. E. D. Stevens, P. Coppens, *Acta Crystallogr., Sect. B: Struct. Sci.*, 1980, **36**, 1864.
17. P. Coppens, *Acta Crystallogr., Sect. A: Found. Crystallogr.*, 1984, **40**, 184.
18. A. Martin, A. A. Pinkerton, *Acta Crystallogr., Sect. B: Struct. Sci.*, 1998, **54**, 471.
19. *APEXII v. 2011.4-1*, Bruker, 2011.
20. R. H. Blessing, *Cryst. Rev.*, 1987, **1**, 3.
21. R. H. Blessing, *J. Appl. Cryst.*, 1989, **22**, 396.
22. R. H. Blessing, *Acta Crystallogr., Sect. A: Found. Crystallogr.*, 1995, **51**, 33.
23. G. M. Sheldrick, *Acta Crystallogr., Sect. A: Found. Crystallogr.*, 2008, **64**, 112.
24. N. K. Hansen, P. Coppens, *Acta Crystallogr., Sect. A: Found. Crystallogr.*, 1978, **34**, 909.
25. A. Volkov, P. Macchi, L. J. Farrugia, C. Gatti, P. Mallinson, T. Richter, T. Koritsanszky, *XD2006, Rev. 5.34*, University at Buffalo, State University of New York, Buffalo (NY), 2006.
26. P. J. Becker, P. Coppens, *Acta Crystallogr., Sect. A: Found. Crystallogr.*, 1974, **30**, 129.
27. F. L. Hirschfeld, *Acta Crystallogr., Sect. A: Found. Crystallogr.*, 1976, **32**, 239.
28. A. I. Stash, V. G. Tsirelson, *Acta Crystallogr., Sect. A: Found. Crystallogr.*, 2002, **35**, 371.
29. A. I. Stash, V. G. Tsirelson, *Crystallogr. Rep.*, 2005, **50**, 177.

30. R. Dovesi, V. R. Saunders, C. Roetti, R. Orlando, C. M. Zicovich-Wilson, F. Pascale, B. Ci-valleri, K. Doll, N. M. Harrison, I. J. Bush, P. D´Arco, M. Llunell, *CRYSTAL09* (*CRYSTAL09 User´s Manual*), University of Torino, Torino, 2009.
31. C. M. Zicovich-Wilson, M. L. San-Román, M. A. Camblor, F. Pascale, J. S. Durand-Niconoff, *J. Am. Chem. Soc.*, 2007, **129**, 11512.
32. M. V. Vener, A. V. Manaev, V. G. Tsirelson, *J. Phys. Chem. A*, 2008, **112**, 13628.
33. A. V. Shishkina, V. V. Zhurov, A. I. Stash, M. V. Vener, A. A. Pinkerton, V. G. Tsirelson, *Cryst. Growth Des.*, 2013, **13**, 816.
34. M. Currie, J. C. Speakman, N. A. Curry, *J. Chem. Soc. A*, 1967, 1862.
35. G. Portalone, M. Colapietro, *Acta Crystallogr.*, *Sect. E: Struct. Rep. Online*, 2006, **62**, o4725.
36. F. H. Allen, O. Kennard, D. G. Watson, *J. Chem. Soc.*, *Perkin Trans. 2*, 1987, S1.
37. V. G. Tsirelson, *Kvantovaya khimiya. Molekuly, molekulyarnye sistemy i tverdye tela* [*Quantum Chemistry. Molecules, Molecular Systems, and Solids*], Binom, Moscow, 2010, 496 pp. (in Russian).
38. V. G. Tsirelson, E. V. Bartashevich, A. I. Stash, V. A. Potemkin, *Acta Crystallogr., Sect. B: Struct. Sci.*, 2007, **63**, 142.
39. E. V. Bartashevich, D. K. Nikulov, M. V. Vener, V. G. Tsirelson, *Comput. Theor. Chem.*, 2011, **973**, 33.
40. S. T. Howard, O. Lamarche, *J. Phys. Org. Chem.*, 2003, **16**, 133.
41. J. Cioslowski, S. T. Mixon, *J. Amer. Chem. Soc.*, 1991, **113**, 4142.
42. I. Mata, I. Alkorta, E. Espinosa, E. Molins, *Chem. Phys. Lett.*, 2011, **507**, 185.
43. M. V. Vener, A. N. Egorova, A. V. Churakov, V. G. Tsirelson, *J. Comp. Chem.*, 2012, **33**, 2303.
44. D. A. Kirzhnits, *J. Exp. Theor. Phys.* (*Engl. Transl.*), 1957, **5**, 64 [*Zh. Eksperim. Teor. Fiziki*, 1957, **5**, 115].
45. S. Luo, *Int. J. Theor. Phys.*, 2002, **41**, 1713.
46. H. J. Bohórquez, R. Boyd, *Theor. Chem. Acc.*, 2010, **127**, 393.
47. H. J. Bohórquez, C. F. Matta, R. J. Boyd, *Int. J. Quantum Chem.*, 2010, **110**, 2418.
48. H. J. Bohórquez, R. J. Boyd, C. F. Matta, *J. Phys. Chem.*, 2011, **115**, 12991.
49. S. Shaik, D. Danovich, Wei Wu, P. C. Hiberty, *Nat. Chem.*, 2009, **1**, 443.
50. S. J. Grabowski, *Chem. Rev.*, 2011, **111**, 2597.
51. J. Overgaard, B. B. Iversen, in *Structure and Bonding*, Ed. D. Stalke, Springer, Heidelberg—New York—Dordrecht—London, 2012, p. 53.
52. T. Clark, M. Hennemann, J. S. Murray, P. Politzer, *J. Mol. Model.*, 2007, **13**, 291.
53. Z. P. Shields, J. S. Murray, P. Politzer, *Int. J. Quantum. Chem.*, 2010, **110**, 2823.
54. P. Politzer, J. S. Murray, T. Clark, *Phys. Chem. Chem. Phys.*, 2010, **12**, 7748.
55. J. S. Murray, P. Lane, T. Clark, K. E. Riley, P. Politzer, *J. Mol. Model.*, 2012, **18**, 541.

*Received June 6, 2013;*
*in revised form July 18, 2013*